

pubs.acs.org/JPCC Article

An Insight into the Mechanism of Alkyl Side-Chain Engineering of BTCN on Its Photovoltaic Properties—A Theoretical Study

Wencheng Li,[§] Zhijun Cao,[§] Jiaman Peng, Heidi P. Hendrickson, and Shaohui Zheng*



Cite This: https://doi.org/10.1021/acs.jpcc.4c02780



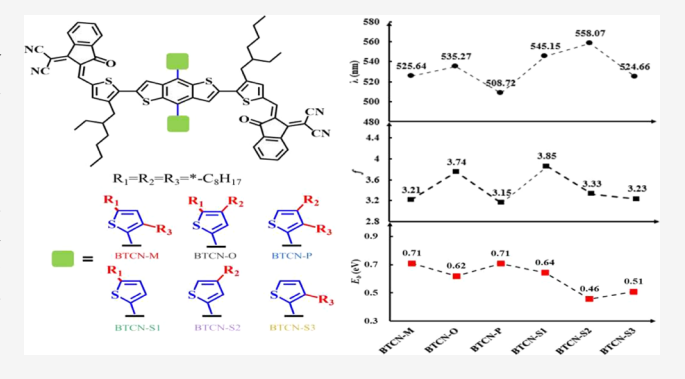
ACCESS I

III Metrics & More

Article Recommendations

s Supporting Information

ABSTRACT: Organic photovoltaic materials featuring thiophene-substituted benzo[1,2-b:4,5-b']dithiophene (BDT-T) units show great potential. However, the influence of alkyl side-chain engineering on BDT-T units in these materials remains elusive. In this study, we focused on a high-performance small-molecule BTCN series with an acceptor—donor—acceptor architecture, where BDT-T serves as the donor. We systematically explored how varying the number and positions of alkyl chains on lateral thiophene rings affects the photovoltaic properties. The geometric parameters and ground and excited state properties were calculated using density functional theory (DFT) and time-dependent DFT (TDDFT). The experimentally observed differences in photovoltaic performance between BTCN-M and BTCN-O due to



different substituted positions of the two alkyl chains can be explained well by our calculated data. Furthermore, the results show that, out of the BTCN series considered, BTCN-S1 in which the single-alkyl substitution is next to the sulfur atom of the lateral thiophene molecule could be a promising donor since it has the most negative average electrostatic potential and strongest light absorption in the visible region. Lastly, compared to double-alkyl-chain substitutions, single-chain substitution on the BDT-T unit can decrease the exciton binding energy but may increase the singlet—triplet energy differences in BTCNs. These findings offer valuable insights into alkyl side-chain engineering for optimizing BDT-T-based organic materials.

1. INTRODUCTION

Developing new solar energy materials is crucial for sustainable human development. Compared to traditional silicon solar cells, organic solar cells (OSCs) are known for their flexibility, lightweight, and roll-to-roll production, sparking global researchers' interest. Presently, the power conversion efficiency (PCE) of single-junction OSC has reached 19.9%. In bulk-heterojunction (BHJ) OSCs, the active layers can contain polymer or small-molecule donor and acceptor materials, leading to four types of OSCs. The maximum PCE of ASM OSCs has reached 18%, which is still lower than that of polymer-based OSCs. Since small molecules offer clear molecular structures, easy synthesis, purification, modifiability, and no batch-to-batch variation, selection in the OSC field.

There are several types of small-molecule materials, including oligothiophenes, ¹³ benzodithiophenes (BDTs), ¹⁴ naphthodithiophenes (NDTs), ¹⁵ porphyrins, etc. ^{16,17} Among them, BDT is often used as the core building block for high-performance photovoltaic materials with an acceptor—donor—acceptor (A-D-A) molecular framework. The BDT unit was first introduced by Hou et al. in 2008. ¹⁸ It features a rigid conjugated planar structure and multiple reaction sites, as shown in Figure 1a. Therefore, BDT-based materials have

tunable molecular energy levels and optical gaps, as well as high hole mobility.¹⁹

In BDT-based materials, small, luminescent π -bridges such as benzene and thiophene rings are commonly introduced to modulate the conjugated backbones. These bridges influence the conformation, altering light absorption, energy levels, hole mobility, and blend morphology. By incorporation of π -bridges, photovoltaic materials with diverse properties can be designed. The introduction of thiophene, compared to benzene, not only adjusts energy levels but also boosts intermolecular interactions, fostering π - π stacking and charge transfer. This stems from sulfur's larger atomic radii, facilitating polarization and stronger interactions between sulfur atoms. Furthermore, the introduction of thiophene enables 2D conjugation in BDT-containing molecules. For instance, lateral thiophene rings attached to BDT units facilitate electron delocalization, promoting two-dimensional

Received: April 29, 2024 **Revised:** July 23, 2024 **Accepted:** July 25, 2024



Figure 1. (a) BDT and BDT-T comparison; (b) molecular structures of BTCN series (BTCN-M and BTCN-O in the figure have been synthesized experimentally, and others are newly designed in this work. $R_1 = R_2 = R_3 = n$ -octyl).

 π -conjugation, as shown in Figure 1a. This enhances $\pi - \pi$ stacking, exciton diffusion, and charge transport. Consequently, BDT-T-based ASM OSCs have achieved a PCE of up to 16.0%. ²³

Among BDT-T-based small-molecule materials, Liu et al. designed two A-D-A molecules BTCN-M and BTCN-O, utilizing thiophene as a π -bridge linking two electron-withdrawing 2-(3-oxo-2,3-dihydro-1H-inden-1-ylidene)-malononitrile (DCI) groups, as shown in Figure 1b.²⁴ DCI's electron-withdrawing carbonyl and cyano groups lower LUMO levels.²⁵ Despite similar structures, BTCN-M and BTCN-O differ in alkyl chain positions on BDT-T's thiophene rings: BTCN-O has two octyls at 1,2-positions, while BTCN-M's are at 1,3-positions. These subtle changes significantly affect photovoltaic properties, with BTCN-O excelling as a donor with PC71BM and BTCN-M as an acceptor with PBDB-T.²⁶

Currently, there are limited reports exploring the mechanism of side-chain regulation in ASM OSCs. The reported research includes the substitutions of alkoxy or alkylthiol, 27-29 the adjustment of length of side chain, 30,31 the change of number of side chains,³² the different position of substitutions of side chains, 33,34 the change of position and size of branched chain,³⁵ and the addition of phenyl or thiophenyl.^{36–38} Initially, researchers introduced alkyl side chains to improve their solubility.³⁹ Later, researchers found that as charge transfer occurs through the delocalization of π -electrons on conjugated skeleton, which is largely limited by the effective conjugation length, the substitution position of alkyl side chains can precisely adjust the steric hindrance effect, thus impacting the effective conjugation length and charge carrier mobility.⁴⁰ However, the mechanisms by which alkyl side chains regulate photovoltaic properties remain not very clear, especially regarding how they influence A-D-A small-molecule interconversion from electron donor to acceptor, which is currently underexplored.

To investigate the effects of the position and number of alkyl side chains on the photovoltaic properties of A-D-A-type small molecules, we designed four new molecules based on the existing BTCN series (BTCN-M/O), as shown in Figure 1b. These molecules comprise the double-chain-substituted BTCN-P and single-chain-substituted molecules BTCN-S1,

BTCN-S2, and BTCN-S3. In BTCN-M, two octyl chains are introduced at the 2- and 3-positions of the thiophene units of BDT-T. Conversely, BTCN-S1, S2, and S3 feature a single octyl chain at the 1-, 2-, and 3-positions, respectively. We have employed density functional theory (DFT) and time-dependent DFT (TDDFT) to calculate photoelectric properties of the BTCN series, including molecular planarity, dipole moments, frontier molecular orbitals, electrostatic potentials, electron—hole distributions, UV—visible absorption spectra, exciton binding energies, as well as singlet—triplet energy difference.

2. COMPUTATIONAL DETAILS

GaussView 5.0 was used for molecular modeling. ⁴¹ DFT and TDDFT calculations were carried out using Gaussian 2009 Rev E.01⁴² software packages. In order to simulate the environment in experiment, an integral equation formalism variant polarizable continuum model (IEF-PCM) was applied. ⁴³ We chose chloroform (CF) as the solvent with a relative dielectric constant of $\varepsilon = 4.71$ for keeping consistent with the experiment. ²⁴

Benchmark calculations were run to test the various levels of theory by comparing the calculated energy of frontier molecular orbitals (FMOs) and absorption peaks in the visible region to experimental results of BTCN-M/O.²⁴ Density functionals considered include pure density functional PBE, 44 classical hybrid density functional B3LYP,45 and long-range corrected (LRC) density functionals CAM-B3LYP, 40 ω B97X, ⁴⁷ and ω B97XD. ⁴⁸ Likewise, multiple basis sets were also considered, including 6-31G(d), 6-311+G(d), 6-311G(d), 6-311G(d), 6-311G(d,p), Def2TZVP, and Def2TZVPP. For LRC density functionals ω B97X and ω B97XD, we optimized the range separation parameter ω . B3LYP/6-31G(d)/PCM was utilized for geometry optimizations of ground state since this combination has been proved capable of reproducing experimental geometry well.^{49,50} Frequency calculations were also run to confirm that there is no imaginary frequency. Previous calculations have shown that, after parameter optimization, $\omega B97X$ and $\omega B97XD$ can predict ionization potential (IP), electron affinity (EA), excited state energy level, and other properties in good agreement with experimental values.⁵¹ This is because LRC density functionals can partly

solve the derivative discontinuity problem and self-interaction error, whereas traditional density functional often leads to inaccurate and underestimated FMO gaps. ⁵²

The ω parameter optimization method is as follows:⁴⁸

$$J^{2}(\omega) = J_{N}^{2}(\omega) + J_{N+1}^{2}(\omega)$$
(1)

$$J_N^2(\omega) = [E_{\text{HOMO}}^{\omega}(N) + E^{\omega}(N-1) - E^{\omega}(N)]^2$$
 (2)

$$J_{N+1}^{2}(\omega) = \left[E_{\text{HOMO}}^{\omega}(N+1) + E^{\omega}(N) - E^{\omega}(N+1)\right]^{2}$$
(3)

where $E^{\omega}_{\text{HOMO}}(N)$ is the highest occupied molecular orbital (HOMO) energy of N electron system; $E^{\omega}(N)$ is the total energy of N electron system; and N, N-1, and N+1, respectively, represent neutral, cation, and anion states. The optimized values of ω for BTCN-M and BTCN-O are 0.01 and 0.03 for the ω B97X functional and 0.03 and 0.02 for the ω B97XD functional, respectively, as shown in Figure S1.

Exciton binding energy (E_b) is the energy required to separate excited electron—hole pair into free electrons and holes.⁵³ The excitons generated by photoexcitation in organic materials are generally Frenkel excitons, so E_b is typically around 0.1–1 eV.⁵⁴ E_b is an important factor affecting the photovoltaic properties of organic materials because those with small E_b usually show better charge separation efficiency.⁵⁴ In this work, E_b was calculated by using the CAM-B3LYP functional and Def2TZVP basis set according to the following equations:⁵⁵

$$E_{\rm b} = E_{\rm fund} - E_{\rm opt} \tag{4}$$

$$E_{\text{fund}} = IP - EA$$
 (5)

$$IP = E(N-1) - E(N)$$
(6)

$$EA = E(N) - E(N+1) \tag{7}$$

$$E_{\text{opt}} = E(N, \text{ excited}) - E(N)$$
 (8)

where $E_{\rm fund}$ is fundamental gap energy; $E_{\rm opt}$ denotes optical gap energy, which is the vertical excitation energy from ground state (S₀) to the first excited singlet state (S₁) obtained by TDDFT calculation; IP means the ionization potential; and EA is the electron affinity.

In addition, we carried out TDDFT calculations for BTCN series at the CAM-B3LYP/Def2TZVP level and used Multiwfn3.7 software package⁵⁶ to generate the UV-vis absorption spectra. To account for the broadening of the peak width that occurs in experimental conditions, the full width at half-maximum (FWHM) of the absorption peak was set to 0.5 eV and Gaussian broadening was applied.

In organic photovoltaic materials, $\Delta E_{\rm ST}$ is the energy difference between the first singlet and first triplet excited states, which can be approximately equal to the sum of $\Delta E_{\rm CT}$ and $\Delta E_{\rm BET}$. ⁵⁷

$$\Delta E_{\rm ST} = E_{\rm S_1} - E_{\rm T_1} = \Delta E_{\rm CT} + \Delta E_{\rm BET} \tag{9}$$

$$\Delta E_{\rm CT} = E_{\rm S_1} - E_{\rm CT} \tag{10}$$

$$\Delta E_{\rm BET} = E_{\rm CT} - E_{\rm T_1} \tag{11}$$

where $\Delta E_{\rm CT}$ represents the driving force of the charge transfer (CT) state, and a smaller $\Delta E_{\rm CT}$ corresponds to a smaller voltage loss and therefore a higher open-circuit voltage. ^{58,59}

The back electron transport (BET) $\Delta E_{\rm BET}$ is the energy difference between $E_{\rm CT}$ and $E_{\rm T_1}$, representing the recombination of the triplet CT exciton to the T₁ state. Decreasing $\Delta E_{\rm BET}$ can reduce the recombination of triplet CT excitons. Thus, a small $\Delta E_{\rm ST}$ can effectively solve the problem of voltage loss and charge recombination in OSCs. 63,64

To further analyze the properties of excited states of these molecules, the intramolecular charge transfer distance $(D_{\rm CT})$ and amount $(q_{\rm CT})$ of S_1 state were calculated with Multiwfn3.7 software package. ⁵⁶

The formula to obtain $D_{\rm CT}$ is as follows: 65,66

$$D_{x} = |X_{\text{ele}} - X_{\text{hole}}| \tag{12}$$

$$D_{y} = |Y_{\text{ele}} - Y_{\text{hole}}| \tag{13}$$

$$D_z = |Z_{\text{ele}} - Z_{\text{hole}}| \tag{14}$$

$$D_{\rm CT} = \sqrt{(D_x)^2 + (D_y)^2 + (D_z)^2}$$
(15)

where $X_{\rm ele}$, $Y_{\rm ele}$, and $Z_{\rm ele}$ represent the X, Y, and Z coordinates of excited electron, respectively, and $X_{\rm hole}$, $Y_{\rm hole}$, and $Z_{\rm hole}$ denote the X, Y, and Z coordinates of the corresponding hole, respectively.

Likewise, $q_{\rm CT}$ means the quantity of charge whose distribution is perturbed during the process of excitation. This amount can be obtained from the following equations:⁶⁶

$$\Delta \rho(r) = \rho_{\rm EX}(r) - \rho_{\rm GS}(r) = \rho^+ + \rho^- \tag{16}$$

$$q_{\rm CT} = \int_0^r \rho^+ dr \tag{17}$$

Here, ρ is the electron density; EX/GS means excited/ground state, respectively; and $\Delta \rho$ is the electron density difference during the excitation, and can be divided into positive ρ^+ and negative ρ^- parts. Electron—hole distribution diagrams of the S₁ states of the six BTCN molecules were generated using the Multiwfn3.7⁵⁶ and IQmol software packages.⁶⁷ In addition, electrostatic potential (ESP) diagrams were also created using the Multiwfn3.7 software package.⁵⁶

The fluorescence quantum yield of BDT and BDT-T was also calculated with the B3LYP/6-31G(d)/PCM theory level. We calculated radiative transition rate $(k_{\rm r})$ and nonradiative transition rate $(k_{\rm ic})$ with MOMAP-2021A software package. ^{68,69}

3. RESULTS AND DISCUSSION

In this section, we first discuss benchmark calculations. Then, we compare the molecular geometry parameters and ground state electronic structures of the BTCN series. Next, the photovoltaic properties including electronic absorption spectra, $E_{\rm b}$, $\Delta E_{\rm ST}$, electron—hole distributions of S₁ state, and ESP are presented and discussed.

3.1. Benchmark Calculations. In the initial molecular modeling for this study, all possible orientations and configurations of the BTCN series of molecules were tested. For example, the side thiophene of the BDT-T unit could adopt multiple rotational configurations in these molecules. Geometry optimizations were carried out for all six molecules, and the configurations that have the lowest energy were selected as the ground state structures, as shown in Figure S2.

In order to determine the level of theory best suited to the BTCN series, we first performed benchmark calculations. The

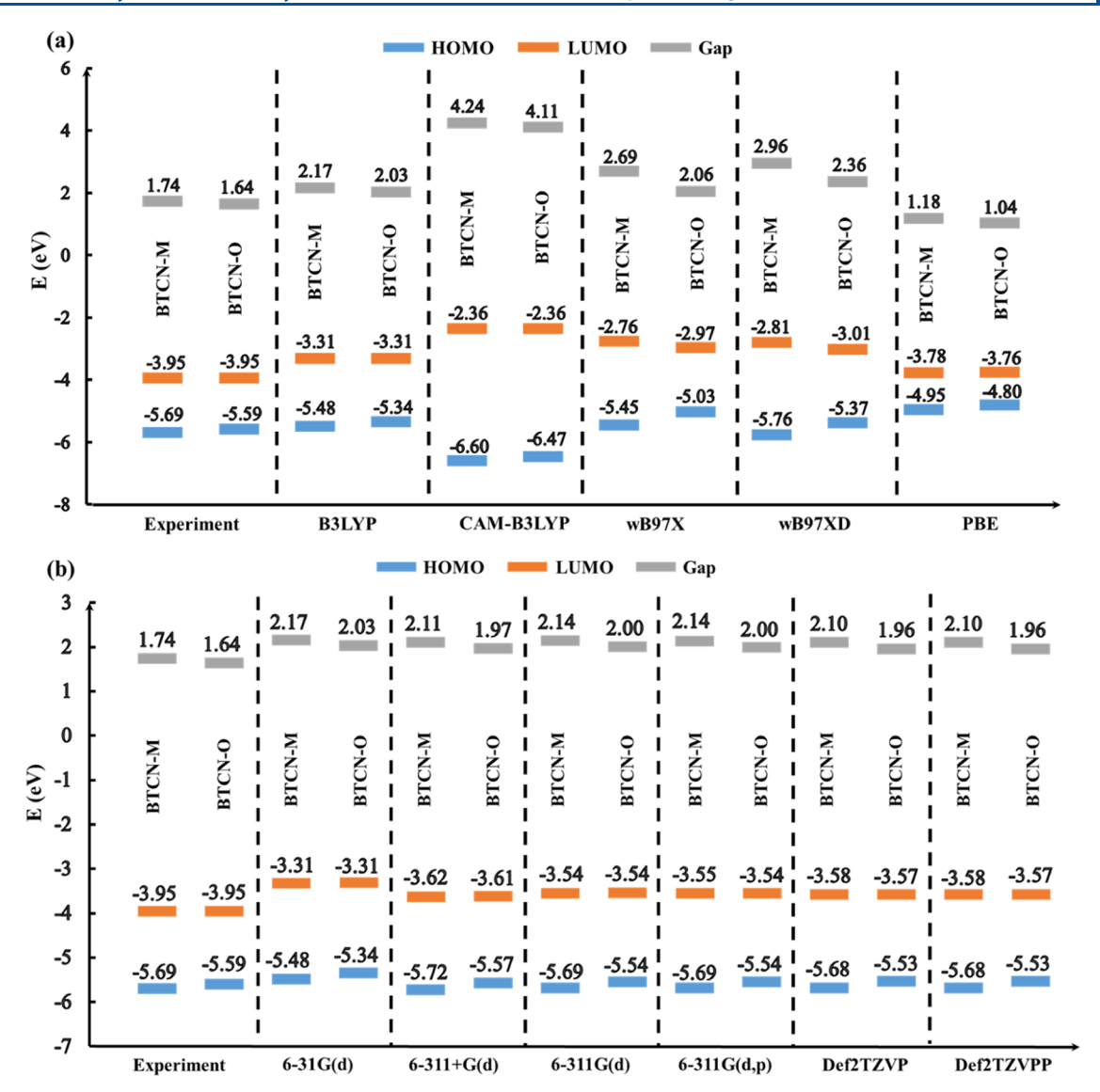


Figure 2. Comparisons between experimental and calculated FMOs. (a) Effects of density functionals: B3YLP, CAM-B3LYP, ωB97XD, and PBE with 6-31G(d) basis sets. (b) Effects of basis sets: 6-31G(d), 6-311+G(d), 6-311G(d), 6-311G(d,p), Def2TZVP, and Def2TZVPP with the B3LYP density functional. For all calculations, IEF-PCM (chloroform) was employed.

FMO energy and wavelength of main absorption peaks of BTCN-M and BTCN-O have been calculated with different levels of theory and then compared to the experimental values, 24 as shown in Figures 2 and 3. Multiple density functionals, including PBE, B3YLP, CAM-B3LYP, ω B97X, and ω B97XD, were used to calculate the FMO energy for BTCN-M and BTCN-O with the 6-31G(d) basis set, as shown in Figure 2a. The FMO energy calculated using the B3LYP functional was in best agreement with the experimental values, which is consistent with previous reports since B3LYP often can reproduce experimental energy of FMO due to error cancellation. 49,50

The effects of basis sets were also considered, as presented in Figure 2b. Six basis sets including 6-31G(d), 6-311+G(d), 6-311G(d), 6-311G(d,p), Def2TZVP, and Def2TZVPP with the B3LYP functional are used. Notably, Figure 2b reveals that both Def2TZVP and Def2TZVPP exhibit superior performance, as their calculated outcomes align most closely with the experimental benchmark. In order to save computational cost,

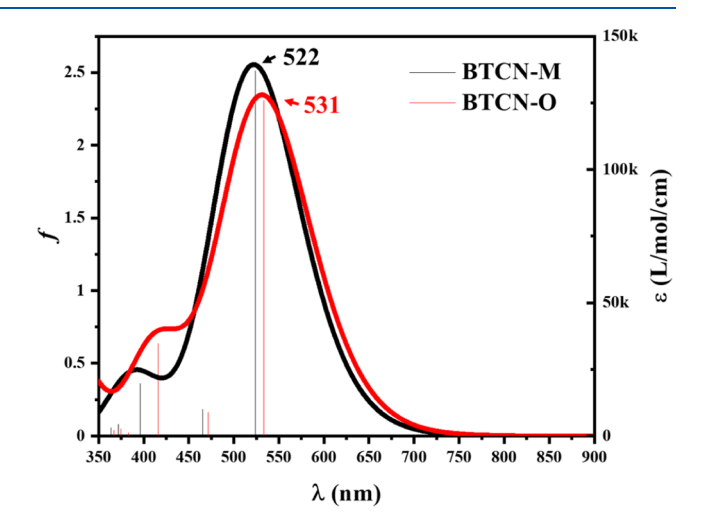


Figure 3. Simulated absorption spectrum of BTCN-M and BTCN-O with the CAM-B3LYP/Def2TZVP/PCM theory level. The fwhm is set to 0.5 eV in the simulation of absorption spectrum.

the Def2TZVP basis set was selected for the rest of the calculations.

In addition to predicting accurate FMO energies, the calculations also correctly reproduce the experimental trend of FMO energy between BTCN-M and BTCN-O. For instance, the calculated HOMO energy of BTCN-M is lower, and the calculated FMO gap energy is higher than those of BTCN-O, which is consistent with the experiments. On the other hand, the FMO energy measured in the experiment actually refers to the change of free energy due to gaining (acceptor) and losing (donor) an electron at room temperature, which is not completely consistent with the changes of SCF energy at 0 K calculated with DFT. We also have calculated the changes of free energy due to gaining and losing an electron at room temperature, as shown in Table S1, but this does not improve the accuracy of these values, so we still use the calculated HOMO/LUMO energy.

The calculated wavelengths of the main absorption peaks of BTCN-M and BTCN-O in chloroform were also compared to the experiments to determine the appropriate level of theory for excited state properties. The density functionals PBE, B3YLP, CAM-B3LYP, ω B97X, and ω B97XD with the 6-31G(d) basis set are considered, as shown in Table S2. Surprisingly, only the CAM-B3LYP functional reproduces the experimentally observed red shift of the main absorption peaks between BTCN-M (622 nm) and BTCN-O (626 nm).²⁴ In addition, the effect of the basis sets was also tested. As shown in Table S3 and Figure S3, the calculated wavelength (522/531 nm, respectively) of the main absorption peak of BTCN-M and BTCN-O with the Def2TZVP basis set is closer to the experimental values (622 and 626 nm, respectively) than the other five basis sets.²⁴ Since the simulated absorption spectra obtained at the CAM-B3LYP/Def2TZVP/PCM level correctly reproduce the experimental trend, that is, the red shift of absorption peaks from BTCN-M to BTCN-O,24 this level of theory was used for excited state calculations in the rest of this

To summarize, various density functionals and basis sets were rigorously tested against experimental benchmarks. The nuanced impact of distinct alkyl side-chain substitutions on both ground and excited electronic structures underscores the criticality of choosing the appropriate density functional and basis set. Notably, CAM-B3LYP emerged as the sole candidate capable of accurately replicating the experimental trend observed in the absorption peaks of BTCN-M and -O, highlighting the significance of incorporating the LRC exchange-correlation kernel within the hybrid B3LYP framework.

3.2. Geometric Parameters. The four major dihedral angles that determine the planarity of BTCNs, as shown in Figure 4, are presented in Table 1. The averaged values are utilized to represent the planarity of these molecules, where a smaller average value indicates a more planar molecule. The data in Table 1 show that the BTCN-O molecule has the best planarity out of the three double-alkyl-side-chain-substituted molecules, followed by BTCN-M and BTCN-P. This is consistent with the results reported in the literature. Among the three single-alkyl-side-chain-substituted molecules, BTCN-S2 has the best planarity. Overall, the order of planarity of six molecules is BTCN-S2 > S1 > O > M > S3 > P. The substitution at position 3 of the lateral thiophene ring of the BDT-T unit (as shown in Figure 1) greatly decreases the planarity because of the steric hindrance between the alkyl



Figure 4. Four key dihedral angles that determine the planarity of the BTCN series. The lateral thiophene rings (blue) and alkyl side chains (red) at different positions on the lateral thiophene rings are highlighted.

Table 1. Four Major Dihedral Angles and the Averaged Values of the BTCN Series (Unit: Degrees)

	$oldsymbol{arphi}_1$	$arphi_2$	φ_3	$arphi_4$	average
BTCN-M	71.7	70.7	30.5	39.5	53.1
BTCN-O	56.2	55.3	29.4	38.6	44.9
BTCN-P	70.5	77.3	41.2	39.3	57.1
BTCN-S1	54.8	55.8	21.6	39.4	42.9
BTCN-S2	57.7	57.1	36.5	2.3	38.4
BTCN-S3	73.8	73.1	40.1	27.1	53.5

chain and backbone. Not surprisingly, BTCN-M, BTCN-P, and BTCN-S3 all have this type of substitution and thus are the least planar out of the six molecules. Finally, the synergistic effects of the alkyl side chain also affect the planarity of the molecules. In general, the planarity of the double-alkyl side-chain-substituted molecules is worse than that of the single-alkyl side-chain-substituted molecules, except for BTCN-S3.

3.3. FMO Energy and Dipole Moment. Figure 5a shows the FMO and gap energy of the BTCNs. The differences among LUMO energies are quite small (<0.04 eV), but the differences among HOMO energies are quite noticeable (up to 0.21 eV). The larger effect on the HOMO energy is reasonable because the electron distribution of the HOMO is mainly on the donor part of these molecules, which is also where the alkyl side chains are incorporated, but the electron distribution of the LUMO is mainly on the acceptor part of the molecule. For the double- and single-alkyl-side-chain substitutions, the gap energy is generally correlated with the planarity. The orbital gap becomes lower toward better planarity of these molecules, and this is consistent with previous research.⁷⁰ It is the better planarity that is conducive to electron delocalization, resulting in a lower fundamental gap.

The dipole moment is another important property because increasing the dipole moment moderately is conducive to enhance both the self-assembly of organic molecules and the charge carrier mobility. The influences of double- and single-alkyl-side-chain substitution on the molecular dipole moment are quite different. In the double-chain substitutions, the molecules with better planarity have higher dipole moments (BTCN-P, BTCN-M, BTCN-O: 0.45, 0.82, and 1.01). For the single-chain substitutions, the molecules with better planarity have lower dipole moments (BTCN-S3, BTCN-S1, and BTCN-S2: 0.95, 0.76, and 0.68). The difference can be attributed to the difference in the electron-donating ability based on the number of alkyl side chains. Double-alkyl-side-chain substitutions have stronger electron-donating generally;

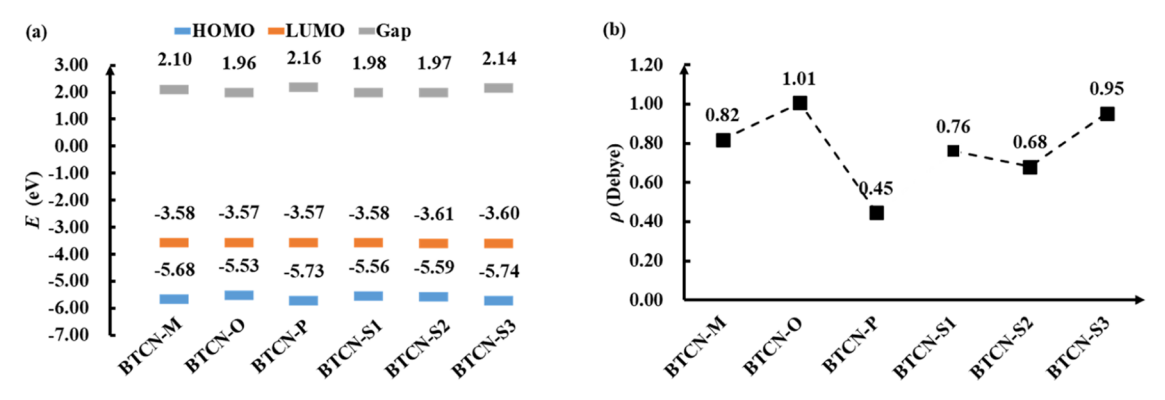


Figure 5. (a) FMO and gap energy of the BTCN series. (b) Dipole moments of the BTCN series. All results are obtained at the B3LYP/Def2TZVP/PCM level.

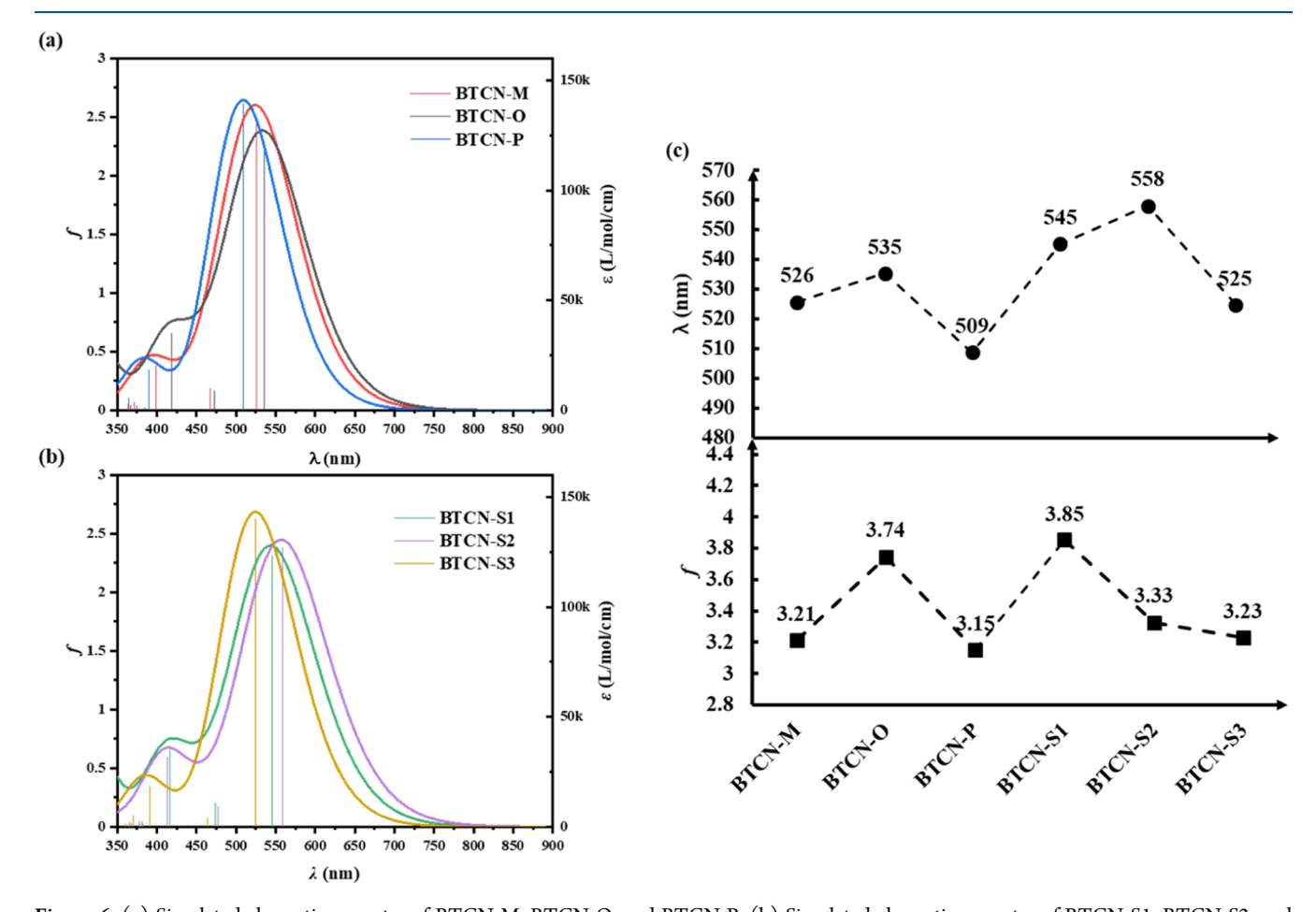


Figure 6. (a) Simulated absorption spectra of BTCN-M, BTCN-O, and BTCN-P. (b) Simulated absorption spectra of BTCN-S1, BTCN-S2, and BTCN-S3. (c) Wavelength of main absorption peaks and total oscillator strength in the visible region. All TDDFT calculations are based on CAM-B3LYP/Def2TZVP/PCM. In the simulation of the absorption spectra, the full width at half-maximum (FWHM) is set to 0.5 eV.

consequently, the donor part of these molecules is more negative due to the better planarity. But this is not the case for single-alkyl-side-chain substitutions.

3.4. Absorption Spectra. The simulated absorption spectra of all six BTCN molecules are provided in Figure 6 and Tables S3 and S4. For double- or single-alkyl-side-chain substitutions, the trends in the main absorption peaks correspond to the trends in the FMO energy gap shown in Figure 5. The wavelengths of the absorption peaks for BTCN-O, BTCN-M, and BTCN-P are 535, 526, and 508 nm, respectively, as shown in Figure 6a. The wavelengths of main

absorption peaks for BTCN-S2, BTCN-S1, and BTCN-S3 are 558, 545, and 525 nm, respectively, as displayed in Figure 6b. Likewise, these trends are opposite to the trends in planarity, as shown in Table 1. The relationship between the peak absorption wavelength and planarity is reasonable because the planarity determines the fundamental gap energy.

Figure 6c illustrates the total oscillator strength of all molecules in the visible region. BTCN-O exhibits a stronger absorption value of 3.74 compared to BTCN-M, which has an absorption of 3.21. This disparity can be attributed to the smaller fundamental gap in BTCN-M, which not only causes a

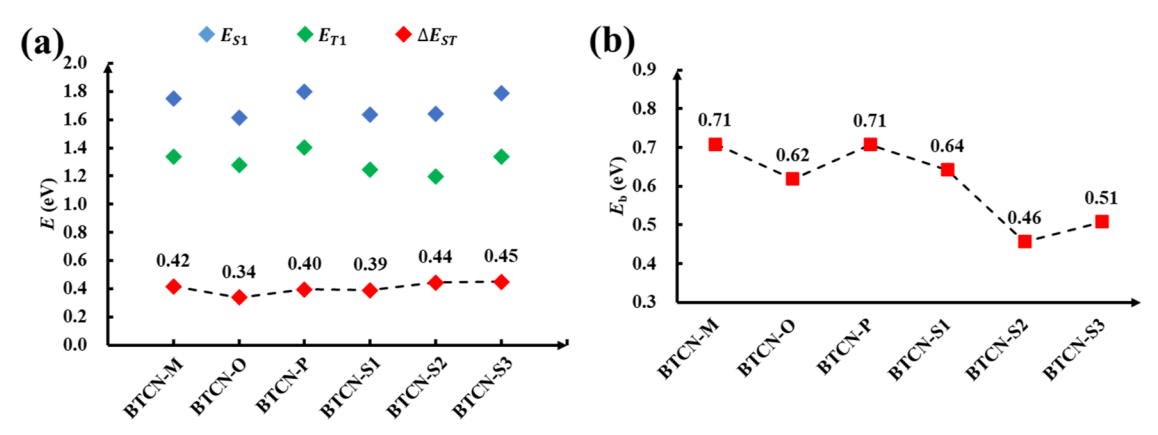


Figure 7. (a) Singlet—triplet energy difference (ΔE_{ST}) and (b) exciton binding energy (E_b) of the set of BTCN molecules. All calculations were obtained at the CAM-B3LYP/Def2TZVP/PCM level of theory.

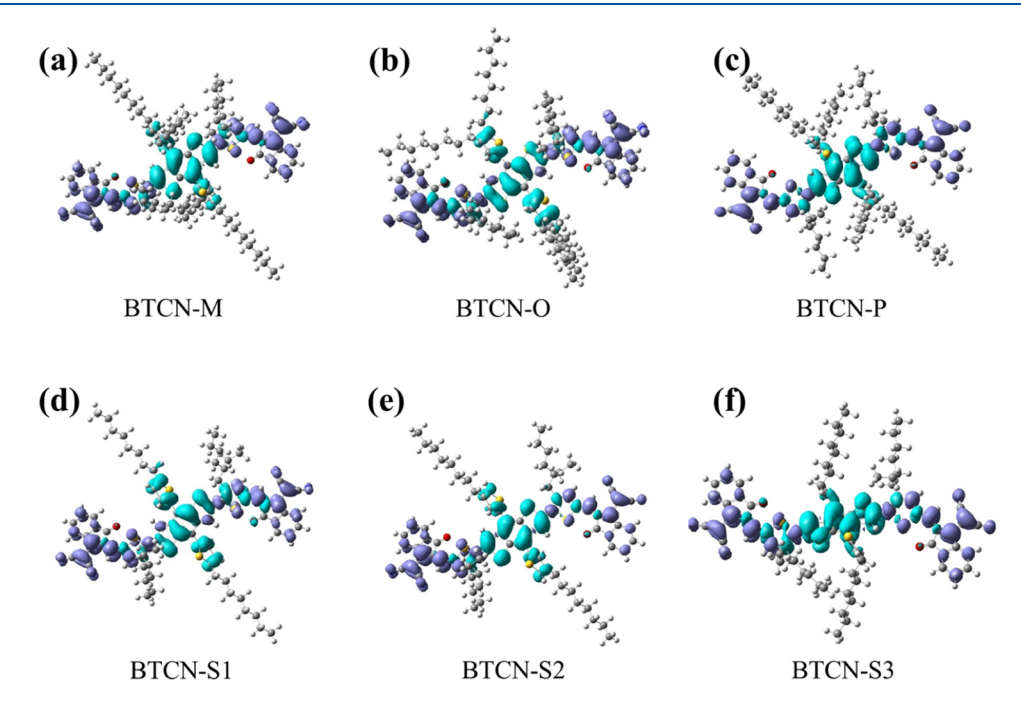


Figure 8. Electron (purple) and hole (green) pair distribution diagram for the first excited state for each BTCN: (a) BTCN-M; (b) BTCN-O; (c) BTCN-P; (d) BTCN-S1; (e) BTCN-S2; (f) BTCN-S3. All results are calculated with CAM-B3LYP/Def2TZVP/PCM.

red shift in the wavelength of the absorption peak but also enhances the oscillator strength due to the stronger coupling between the S₁ excited state and the ground state. In experiment, BTCN-M/O is blended with PC71BM in an actual device,²⁴ and due to the limited light absorption ability of PC71BM,⁷² the absorption in blended devices mainly depends on the BTCN molecules. Indeed, the short-circuit current density of BTCN-O:PC71BM (11.34 mA cm⁻²) is much higher than that of BTCN-M:PC71BM (0.506 mA cm⁻²),⁷³ which is consistent with the calculated absorption strength. On the other hand, BTCN-S1, BTCN-S2, and BTCN-S3 all show stronger absorption strength than BTCN-M. In particular, BTCN-S1 has the strongest absorption strength among the six molecules and the most red-shifted absorption peak with respect to the three double-alkyl-chainsubstituted molecules. In addition, we also presented the fluorescence quantum yields of BDT and BDT-T in Figure 1a and Table S5. Obviously, the introduction of lateral thiophene rings significantly lowers the quantum yield (from 96.28 to

0.00218%). This is favorable for reducing the radiative energy loss.

3.5. Exciton Binding Energy (E_b) and Singlet—Triplet **Energy Differences.** Figure 7 shows the first singlet and triplet excitation energies, ΔE_{ST} 's and E_b 's of the BTCN series. As shown in Figure 7a and Table S6, the ΔE_{ST} of BTCN-O is the smallest among the double-alkyl-side-chain-substituted molecules because it has the smallest value of E_{S_1} due to its best planarity. Overall, the double-alkyl-side-chain substitutions seem able to reduce the $\Delta E_{\rm ST}$ more than the single-alkylside-chain substitutions because they generally have higher values of $E_{\rm T}$, and thus could reduce voltage loss and charge recombination. ΔE_{ST} of BTCN-O is slightly lower than that of BTCN-M, corresponding to the better performance of a BTCN-O-based OSC previously observed in experiment.²⁴ Among the single-alkyl-side-chain substitutions, $\Delta E_{\rm ST}$ of BTCN-S1 is the lowest, followed by BTCN-S2, then BTCN-S3, and the differences are minor. The reason is the differences in $E_{\rm T}$ and molecular planarity. This trend suggests that singlealkyl-side-chain substitutions closer to the sulfur atom of the lateral thiophene ring may be favorable for reducing voltage loss and charge recombination.

The charge separation process in organic materials is generally difficult due to a large exciton binding energy in these molecular systems.⁷⁴ In order to reduce the energy loss during exciton dissociation, it is necessary to reduce the $E_{\rm b}$ of the active-layer material.⁴⁹ Although $E_{\rm b}$ is hard to measure experimentally, Figure 7b and Table S7 show the calculated $E_{\rm b}$ values for the molecules considered in this work. The $E_{\rm h}$ of BTCN-O is 0.62 eV, which is lower than that of BTCN-M (0.71 eV). This can be attributed to the smaller difference between IP and EA of BTCN-O. The result is consistent with the better photovoltaic performance of BTCN-O in experiment again. 24 In general, the $E_{\rm b}$ of single-alkyl-side-chainsubstituted molecules is lower than those of double-alkyl-sidechain-substituted molecules (except for BTCN-O) since they generally have smaller fundamental gaps. Thus, single-alkylside-chain substitution may be more conducive for exciton separation in the BTCN series of molecules.

3.6. Electron–Hole Distribution of the First Excited State and ESP. The excited state properties of the BTCN molecules were also investigated. The electron—hole distributions of the first excited singlet states are listed in Figure 8 and Table 2. The charge transfer amount, q_{CT} , calculated for all

Table 2. Intramolecular Charge Transfer Distance (D_{CT}) , Intramolecular Charge Transfer Amount (q_{CT}) , the First Excited State Energy (E), and Its Oscillator Strength $(f)^a$

	D_{CT} (Å)	q_{CT} (e)	E (eV)	f
BTCN-M	1.18	0.49	2.36	2.50
BTCN-O	1.04	0.49	2.32	2.29
BTCN-P	0.22	0.49	2.44	2.61
BTCN-S1	0.93	0.49	2.27	2.31
BTCN-S2	0.57	0.49	2.22	2.38
BTCN-S3	0.65	0.49	2.36	2.63

^aAll results are calculated with CAM-B3LYP/Def2TZVP/PCM.

BTCNs is the same and thus is not affected by different positions or numbers of alkyl-side-chain substitutions. However, the intramolecular charge transfer distance $D_{\rm CT}$ does depend on the position of the alkyl side substitution.

When the alkyl substitution is adjacent to the sulfur atom of the lateral thiophene ring of the BDT-T unit, as in BTCN-S1, BTCN-O, and BTCN-M, there is a greater charge transfer distance than when the alkyl substitution position is farther from the sulfur atom, as in BTCN-S3, BTCN-S2, and BTCN-P. A greater charge transfer distance makes charge recombination more difficult, and so these trends suggest that alkyl side substitutions near the sulfur atom of the lateral thiophene ring can reduce charge recombination.

In the experiment blending BTCN-M and BTCN-O,24 BTCN-O was observed to act as the electron donor and BTCN-M as the electron acceptor. In order to understand this phenomenon, the electrostatic potentials (ESPs) of the BTCN molecules were also analyzed via the mechanism of intermolecular electric field (IEF).⁷⁵ The driving force of the IEF mechanism is the ESP difference between donor and acceptor, which directly affects the charge separation at the interface. 76,77 The ESP distributions on the surfaces of the BTCN molecules are shown in Figure 9. Although the ESP distribution is similar across the set of BTCN molecules, the average ESP of BTCN-M (-0.076 eV) is slightly less negative than that of BTCN-O (-0.079 eV). The latter has better planarity; consequently, the better delocalization of π electrons lowers ESP. Therefore, in BTCN-M and BTCN-O blend devices, BTCN-M would be expected to act as the acceptor and BTCN-O as the donor. In addition, by comparing trends in ESP (S1 < S2 < O < M < S3 < P) and trends in planarity (S2 < S1 < O < M < S3 < P), the molecules that are more planar tend to have a more negative ESP. However, BTCN-S2 and BTCN-S1 do not conform to this rule, which may be a result of having a single-alkyl side chain that is farther from the molecular backbone unit. BTCN-S1 has the minimum average (-0.091 eV) of electrostatic potential out of the six molecules, and so is predicted to be the best donor molecule in the set of BTCN molecules. On the other hand, BTCN-P is predicted to be a better acceptor than BTCN-M and the other BTCN molecules.

4. CONCLUSIONS

In conclusion, this study systematically investigated the subtle effects of alkyl-side-chain modifications in BDT-T units on the photoelectrical properties of the BTCN series. The calculated data demonstrate that from the perspective of the FMO

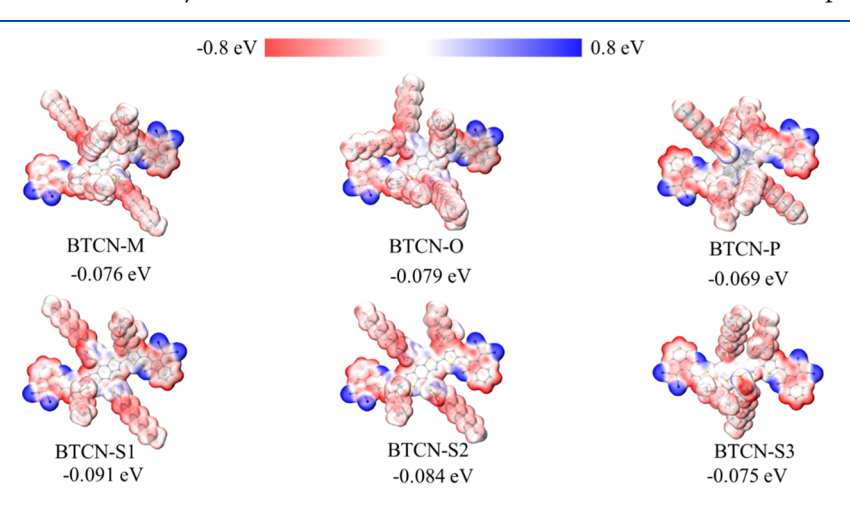


Figure 9. ESP diagrams and the average ESP for each BTCN. The isosurface value is set to 0.001 au. The average of ESP is the average value of all atomic ESPs, calculated with CAM-B3LYP/Def2TZVP/PCM.

energy, absorption intensity, and the average of ESP, the photovoltaic differences between BTCN-M and BTCN-O due to different positions of alkyl-side-chain substitutions can be well explained. The results also show that BTCN-S1 appears to be a promising donor for small-molecule organic photovoltaics because it has the most negative average ESP and the strongest light absorption in the visible region. In addition, when the alkyl-side-chain orientation causes less steric hindrance (as in the BTCN-O or BTCN-S2 molecules), the overall molecule is more planar, which results in a smaller energy gap and a more red-shifted absorption spectrum for the molecule. Finally, compared with single-chain substitution, double-chain substitution can reduce the $\Delta E_{\rm ST}$ in BTCNs, but it also increases the $E_{\rm b}$. These insights provide valuable guidance for alkyl side chain engineering in optimizing BDT-T-based organic materials.

ASSOCIATED CONTENT

Supporting Information

The Supporting Information is available free of charge at https://pubs.acs.org/doi/10.1021/acs.jpcc.4c02780.

Results of TDDFT calculations, FMO energies, and excited state analyses (PDF)

AUTHOR INFORMATION

Corresponding Author

Shaohui Zheng — Chongqing Key Laboratory for Advanced Materials and Technologies of Clean Energies, School of Materials and Energy, Southwest University, Chongqing 400700, China; orcid.org/0000-0002-2547-3985; Email: shaohuizheng@swu.edu.cn

Authors

Wencheng Li — Chongqing Key Laboratory for Advanced Materials and Technologies of Clean Energies, School of Materials and Energy, Southwest University, Chongqing 400700, China

Zhijun Cao – Chongqing Key Laboratory for Advanced Materials and Technologies of Clean Energies, School of Materials and Energy, Southwest University, Chongqing 400700, China

Jiaman Peng – Chongqing Key Laboratory for Advanced Materials and Technologies of Clean Energies, School of Materials and Energy, Southwest University, Chongqing 400700, China

Heidi P. Hendrickson — Chemistry Department, Lafayette College, Easton, Pennsylvania 18042, United States;
orcid.org/0000-0002-5012-738X

Complete contact information is available at: https://pubs.acs.org/10.1021/acs.jpcc.4c02780

Author Contributions

[§]W.L. and Z.C. are co-first author.

Notes

The authors declare no competing financial interest.

ACKNOWLEDGMENTS

S.Z. gratefully thanks the Natural Science Foundation of Chongqing, China (cstc2021jcyj-msxmX0964), and the financial support from the Start-up Funding from Southwest University. H.P.H. acknowledges that computational resources were provided in part by the MERCURY consortium (https://

mercuryconsortium.org/) under NSF grants CHE-1229354, CHE-1662030, and CHE-2018427. S.Z. thanks HZWTECH for providing computation facilities.

REFERENCES

- (1) Yao, M. N.; Li, T. F.; Long, Y. B.; Shen, P.; Wang, G. X.; Li, C. L.; Liu, J. S.; Guo, W. B.; Wang, Y. F.; Shen, L.; Zhan, X. W. Color and transparency-switchable semitransparent polymer solar cells towards smart windows. *Sci. Bull.* **2020**, *65* (3), 217–224.
- (2) Mahmood, A.; Wang, J. L. Machine learning for high performance organic solar cells: current scenario and future prospects. *Energy Environ. Sci.* **2021**, *14* (1), 90–105.
- (3) Jia, Z. R.; Qin, S. C.; Meng, L.; Ma, Q.; Angunawela, I.; Zhang, J. Y.; Li, X. J.; He, Y. K.; Lai, W. B.; Li, N.; Ade, H.; Brabec, C. J.; Li, Y. F. High performance tandem organic solar cells via a strongly infrared-absorbing narrow bandgap acceptor. *Nat. Commun.* **2021**, *12* (1), No. 178.
- (4) Xie, L.; Song, W.; Ge, J. F.; Tang, B. C.; Zhang, X. L.; Wu, T.; Ge, Z. Y. Recent progress of organic photovoltaics for indoor energy harvesting. *Nano Energy* **2021**, *82*, No. 105770.
- (5) Wan, X. J.; Li, C. X.; Zhang, M. T.; Chen, Y. S. Acceptor-donor-acceptor type molecules for high performance organic photovoltaics chemistry and mechanism. *Chem. Soc. Rev.* **2020**, 49 (9), 2828–2842.
- (6) Guo, C.; Sun, Y.; Wang, L.; Liu, C.; Chen, C.; Cheng, J.; Xia, W.; Gan, Z.; Zhou, J.; Chen, Z.; Zhou, J.; Liu, D.; Guo, J.; Li, W.; Wang, T. Light-induced quinone conformation of polymer donors toward 19.9% efficiency organic solar cells. *Energy Environ. Sci.* **2024**, *17* (7), 2492–2499.
- (7) Gao, Y.; Yang, X.; Wang, W.; Sun, R.; Cui, J.; Fu, Y.; Li, K.; Zhang, M.; Liu, C.; Zhu, H.; Lu, X.; Min, J. High-Performance Small Molecule Organic Solar Cells Enabled by a Symmetric-Asymmetric Alloy Acceptor with a Broad Composition Tolerance. *Adv. Mater.* 2023, 35 (23), No. 2300531.
- (8) Qin, J.; Chen, Z.; Bi, P.; Yang, Y.; Zhang, J.; Huang, Z.; Wei, Z.; An, C.; Yao, H.; Hao, X.; Zhang, T.; Cui, Y.; Hong, L.; Liu, C.; Zu, Y.; He, C.; Hou, J. 17% efficiency all-small-molecule organic solar cells enabled by nanoscale phase separation with a hierarchical branched structure. *Energy Environ. Sci.* **2021**, *14*, 5903–5910.
- (9) Yang, L.; Zhang, S.; He, C.; Zhang, J.; Yao, H.; Yang, Y.; Zhang, Y.; Zhao, W.; Hou, J. New Wide Band Gap Donor for Efficient Fullerene-Free All-Small-Molecule Organic Solar Cells. *J. Am. Chem. Soc.* **2017**, *139* (5), 1958–1966.
- (10) Mishra, A.; Bauerle, P. Small Molecule Organic Semi-conductors on the Move: Promises for Future Solar Energy Technology. *Angew. Chem., Int. Ed.* **2012**, *51* (9), 2020–2067.
- (11) Coughlin, J. E.; Henson, Z. B.; Welch, G. C.; Bazan, G. C. Design and Synthesis of Molecular Donors for Solution-Processed High-Efficiency Organic Solar Cells. *Acc. Chem. Res.* **2014**, 47 (1), 257–270.
- (12) Lin, Y. Z.; Zhan, X. W. Oligomer Molecules for Efficient Organic Photovoltaics. Acc. Chem. Res. 2016, 49 (2), 175–183.
- (13) Duan, T.; Gao, J.; Xu, T.; Kan, Z.; Chen, W.; Singh, R.; Kini, G. P.; Zhong, C.; Yu, D.; Xiao, Z.; Xiao, Z.; Lu, S. Simple organic donors based on halogenated oligothiophenes for all small molecule solar cells with efficiency over 11%. *J. Mater. Chem. A* **2020**, *8* (12), 5843–5847
- (14) Hu, D.; Yang, Q.; Chen, H.; Wobben, F.; Le Corre, V. M.; Singh, R.; Liu, T.; Ma, R.; Tang, H.; Koster, L. J. A.; Duan, T.; Yan, H.; Kan, Z.; Xiao, Z.; Lu, S. 15.34% efficiency all-small-molecule organic solar cells with an improved fill factor enabled by a fullerene additive. *Energy Environ. Sci.* **2020**, *13* (7), 2134–2141.
- (15) Li, H.; Wu, Q.; Zhou, R.; Shi, Y.; Yang, C.; Zhang, Y.; Zhang, J.; Zou, W.; Deng, D.; Lu, K.; Wei, Z. Liquid-Crystalline Small Molecules for Nonfullerene Solar Cells with High Fill Factors and Power Conversion Efficiencies. *Adv. Energy Mater.* **2019**, 9 (6), No. 1803175.
- (16) Wu, Q.; Deng, D.; Zhou, R.; Zhang, J.; Zou, W.; Liu, L.; Wu, S.; Lu, K.; Wei, Z. Modulation of Donor Alkyl Terminal Chains with the

ı

https://doi.org/10.1021/acs.jpcc.4c02780 J. Phys. Chem. C XXXX, XXX, XXX—XXX

- Shifting Branching Point Leads to the Optimized Morphology and Efficient All-Small-Molecule Organic Solar Cells. ACS Appl. Mater. Interfaces 2020, 12 (22), 25100–25107.
- (17) Kan, B.; Kan, Y.; Zuo, L.; Shi, X.; Gao, K. Recent progress on all-small molecule organic solar cells using small-molecule non-fullerene acceptors. *InfoMat* **2021**, *3*, 175–200.
- (18) Hou, J.; Park, M.-H.; Zhang, S.; Yao, Y.; Chen, L.-M.; Li, J.-H.; Yang, Y. Bandgap and Molecular Energy Level Control of Conjugated Polymer Photovoltaic Materials Based on Benzo[1,2-b:4,5-b']-dithiophene. *Macromolecules* **2008**, *41* (16), 6012–6018.
- (19) Yao, H.; Ye, L.; Zhang, H.; Li, S.; Zhang, S.; Hou, J. Molecular Design of Benzodithiophene-Based Organic Photovoltaic Materials. *Chem. Rev.* **2016**, *116* (12), 7397–7457.
- (20) Lin, Y. Z.; Zhao, F. W.; He, Q.; Huo, L. J.; Wu, Y.; Parker, T. C.; Ma, W.; Sun, Y. M.; Wang, C. R.; Zhu, D. B.; Heeger, A. J.; Marder, S. R.; Zhan, X. W. High-Performance Electron Acceptor with Thienyl Side Chains for Organic Photovoltaics. *J. Am. Chem. Soc.* 2016, 138 (14), 4955–4961.
- (21) Huo, L. J.; Hou, J. H.; Zhang, S. Q.; Chen, H. Y.; Yang, Y. A Polybenzo[1,2-b:4,5-b']dithiophene Derivative with Deep HOMO Level and Its Application in High-Performance Polymer Solar Cells. *Angew. Chem., Int. Ed.* **2010**, 49 (8), 1500–1503.
- (22) Li, M. M.; Ni, W.; Wan, X. J.; Zhang, Q.; Kan, B.; Chen, Y. S. Benzo[1,2-b: 4,5-b ']dithiophene (BDT)-based small molecules for solution processed organic solar cells. *J. Mater. Chem. A* **2015**, 3 (9), 4765–4776.
- (23) Wang, Q.; Zhang, X.; Miao, Y.; Jiang, X.; Wang, X.; Zhang, Z.; Lv, Z.; Liu, T.; Zou, B.; Xu, H.; Yang, R.; Kan, Y.; Sun, Y.; Gao, K. Synergy Effect of Symmetry-Breaking and End-Group Engineering Enables 16.06% Efficiency for All-Small-Molecule Organic Solar Cells. *ACS Mater. Lett.* **2024**, *6* (2), 713–719.
- (24) Liu, D. L.; Yang, L. Y.; Wu, Y.; Wang, X. H.; Zeng, Y.; Han, G. C.; Yao, H. F.; Li, S. S.; Zhang, S. Q.; Zhang, Y.; Yi, Y. P.; He, C.; Ma, W.; Hou, J. H. Tunable Electron Donating and Accepting Properties Achieved by Modulating the Steric Hindrance of Side Chains in A-D-A Small-Molecule Photovoltaic Materials. *Chem. Mater.* **2018**, *30* (3), 619–628.
- (25) Lin, Y.; Wang, J.; Zhang, Z.-G.; Bai, H.; Li, Y.; Zhu, D.; Zhan, X. An Electron Acceptor Challenging Fullerenes for Efficient Polymer Solar Cells. *Adv. Mater.* **2015**, 27 (7), 1170–1174.
- (26) Qian, D. P.; Ye, L.; Zhang, M. J.; Liang, Y. R.; Li, L. J.; Huang, Y.; Guo, X.; Zhang, S. Q.; Tan, Z. A.; Hou, J. H. Design, Application, and Morphology Study of a New Photovoltaic Polymer with Strong Aggregation in Solution State. *Macromolecules* **2012**, *45* (24), 9611–9617.
- (27) Revoju, S.; Biswas, S.; Eliasson, B.; Sharma, G. D. Phenothiazine-based small molecules for bulk heterojunction organic solar cells; variation of side-chain polarity and length of conjugated system. *Org. Electron.* **2019**, *65*, 232–242.
- (28) Zou, Y.; Wu, Y.; Yang, H.; Dong, Y. Y.; Cui, C. H.; Li, Y. F. The effect of alkylthio side chains in oligothiophene-based donor materials for organic solar cells. *Mol. Syst. Des. Eng.* **2018**, 3 (1), 131–141.
- (29) Subbiah, J.; Lee, C. J.; Mitchell, V. D.; Jones, D. J. Effect of Side-Chain Modification on the Active Layer Morphology and Photovoltaic Performance of Liquid Crystalline Molecular Materials. ACS Appl. Mater. Interfaces 2021, 13 (1), 1086–1093.
- (30) Barszcz, B.; Kedzierski, K.; Jeong, H. Y.; Kim, T. D. Spectroscopic properties of diketopyrrolopyrrole derivatives with long alkyl chains. *J. Lumin.* **2017**, *185*, 219–227.
- (31) Lim, E. P3HT-Based Polymer Solar Cells with Unfused Bithiophene–Rhodanine-based Nonfullerene Acceptors. *Bull. Korean Chem. Soc.* **2020**, *41* (6), 644–649.
- (32) Oh, S.; Khan, N.; Jin, S. M.; Tran, H.; Yoon, N.; Song, C. E.; Lee, H. K.; Shin, W. S.; Lee, J. C.; Moon, S. J.; Lee, E.; Lee, S. K. Alkyl side-chain dependent self-organization of small molecule and its application in high-performance organic and perovskite solar cells. *Nano Energy* **2020**, *72*, No. 104708.
- (33) Ryu, H. S.; Lee, H. G.; Shin, S.-C.; Park, J.; Kim, S. H.; Kim, E. J.; Shin, T. J.; Shim, J. W.; Kim, B. J.; Woo, H. Y. Terminal alkyl

- substitution in an A–D–A-type nonfullerene acceptor: simultaneous improvements in the open-circuit voltage and short-circuit current for efficient indoor power generation. *J. Mater. Chem. A* **2020**, 8 (45), 23894–23905.
- (34) Yao, X.; Shao, W.; Xiang, X.; Xiao, W.-J.; Liang, L.; Zhao, F.-G.; Ling, J.; Lu, Z.; Li, J.; Li, W.-S. Side chain engineering on a small molecular semiconductor: Balance between solubility and performance by choosing proper positions for alkyl side chains. *Org. Electron.* **2018**, *61*, 56–64.
- (35) Zhou, R.; Jiang, Z.; Shi, Y.; Wu, Q.; Yang, C.; Zhang, J.; Lu, K.; Wei, Z. Moving Alkyl-Chain Branching Point Induced a Hierarchical Morphology for Efficient All-Small-Molecule Organic Solar Cells. *Adv. Funct. Mater.* **2020**, *30* (51), No. 2005426.
- (36) Qiu, B.; Chen, Z.; Qin, S.; Yao, J.; Huang, W.; Meng, L.; Zhu, H.; Yang, Y.; Zhang, Z.-G.; Li, Y. Highly Efficient All-Small-Molecule Organic Solar Cells with Appropriate Active Layer Morphology by Side Chain Engineering of Donor Molecules and Thermal Annealing. *Adv. Mater.* **2020**, *32* (21), No. 1908373.
- (37) Zeng, A.; Pan, M.; Lin, B.; Lau, T.-K.; Qin, M.; Li, K.; Ma, W.; Lu, X.; Zhan, C.; Yan, H. A Nonfullerene Acceptor with Alkylthio-and Dimethoxy-Thiophene-Groups Yielding High-Performance Ternary Organic Solar Cells. *Sol. RRL* **2020**, *4* (1), No. 1900353.
- (38) Zhang, X.; Wang, Q.; Liang, Z.; Li, M.; Geng, Y. Low-bandgap non-fullerene acceptors based on selenophene π spacer and alkylated indaceno [1,2-b:5,6-b'] dithiophene for organic solar cells. *Org. Electron.* **2019**, *69*, 200–207.
- (39) Mo, D. Z.; Chen, H.; Zhou, J. D.; Tang, N. N.; Han, L.; Zhu, Y. L.; Chao, P. J.; Lai, H. J.; Xie, Z. Q.; He, F. Alkyl chain engineering of chlorinated acceptors for elevated solar conversion. *J. Mater. Chem. A* **2020**, *8* (18), 8903–8912.
- (40) Lei, T.; Wang, J.-Y.; Pei, J. Roles of Flexible Chains in Organic Semiconducting Materials. *Chem. Mater.* **2014**, *26* (1), 594–603.
- (41) Dennington, R. K.; Millam, T. J. GaussView Version 5; Gaussian Inc.: Wallingford, CT, 2009.
- (42) Frisch, M. J.; Trucks, G. W.; Schlegel, H. B.; Scuseria, G. E.; Robb, M. A.; Cheeseman, J. R.; Scalmani, G.; Barone, V.; Petersson, G. A.; Nakatsuji, H.et al. *Gaussian 09*; Gaussian, Inc.: Wallingford, CT, 2013.
- (43) Tomasi, J.; Mennucci, B.; Cammi, R. Quantum mechanical continuum solvation models. Chem. Rev. 2005, 105 (8), 2999–3093.
- (44) Perdew, J. P.; Burke, K.; Ernzerhof, M. Generalized gradient approximation made simple. *Phys. Rev. Lett.* **1996**, 77 (18), 3865–3868.
- (45) Stephens, P. J.; Devlin, F. J.; Chabalowski, C. F.; Frisch, M. J. Ab-Initio Calculation of Vibrational Absorption and Circular-Dichroism Spectra Using Density-Functional Force-Fields. *J. Phys. Chem. A* 1994, 98 (45), 11623–11627.
- (46) Yanai, T.; Tew, D. P.; Handy, N. C. A new hybrid exchange-correlation functional using the Coulomb-attenuating method (CAM-B3LYP). *Chem. Phys. Lett.* **2004**, 393 (1–3), 51–57.
- (47) Chai, J. D.; Head-Gordon, M. Systematic optimization of longrange corrected hybrid density functionals. *J. Chem. Phys.* **2008**, *128* (8), No. 084106.
- (48) Chai, J. D.; Head-Gordon, M. Long-range corrected hybrid density functionals with damped atom-atom dispersion corrections. *Phys. Chem. Chem. Phys.* **2008**, *10* (44), 6615–6620.
- (49) Qiu, W. K.; Zheng, S. H. Designing and Screening High-Performance Non-Fullerene Acceptors: A Theoretical Exploration of Modified Y6. *Sol. RRL* **2021**, *5* (5), No. 2100023.
- (50) Zhang, J.; Xiang, Y.; Zheng, S. From Y6 to BTPT-4F: a theoretical insight into the influence of the individual change of fused-ring skeleton length or side alkyl chains on molecular arrangements and electron mobility. *New J. Chem.* **2021**, *45* (27), 12247–12259.
- (51) Iikura, H.; Tsuneda, T.; Yanai, T.; Hirao, K. A long-range correction scheme for generalized-gradient-approximation exchange functionals. *J. Chem. Phys.* **2001**, *115* (8), 3540–3544.
- (52) Grimme, S.; Hansen, A.; Brandenburg, J. G.; Bannwarth, C. Dispersion-Corrected Mean-Field Electronic Structure Methods. *Chem. Rev.* **2016**, *116* (9), 5105–5154.

- (53) Wannier, G. H. The structure of electronic excitation levels in insulating crystals. *Phys. Rev.* **1937**, 52 (3), 0191–0197.
- (54) Kraner, S.; Scholz, R.; Koerner, C.; Leo, K. Design Proposals for Organic Materials Exhibiting a Low Exciton Binding Energy. *J. Phys. Chem. C* **2015**, *119* (40), 22820–22825.
- (55) Zhang, J.; Peng, S. P.; Wei, Y. C.; Zheng, S. H. A theoretical study of the absorption spectra of electron-deficient pentacene derivatives using DFT and TDDFT. *Spectrochim. Acta, Part A* **2020**, 225, No. 117480.
- (56) Lu, T.; Chen, F. W. Multiwfn: A multifunctional wavefunction analyzer. *J. Comput. Chem.* **2012**, 33 (5), 580–592.
- (57) Chen, X. K.; Wang, T. H.; Bredas, J. L. Suppressing Energy Loss due to Triplet Exciton Formation in Organic Solar Cells: The Role of Chemical Structures and Molecular Packing. *Adv. Energy Mater.* **2017**, 7 (15), No. 1602713.
- (58) Eisner, F. D.; Azzouzi, M.; Fei, Z. P.; Hou, X. Y.; Anthopoulos, T. D.; Dennis, T. J. S.; Heeney, M.; Nelson, J. Hybridization of Local Exciton and Charge-Transfer States Reduces Nonradiative Voltage Losses in Organic Solar Cells. *J. Am. Chem. Soc.* **2019**, *141* (15), 6362–6374.
- (59) Xu, Y.; Yao, H. F.; Ma, L. J.; Wang, J. W.; Hou, J. H. Efficient charge generation at low energy losses in organic solar cells: a key issues review. *Rep. Prog. Phys.* **2020**, *83* (8), No. 082601.
- (60) Rao, A.; Chow, P. C. Y.; Gelinas, S.; Schlenker, C. W.; Li, C. Z.; Yip, H. L.; Jen, A. K. Y.; Ginger, D. S.; Friend, R. H. The role of spin in the kinetic control of recombination in organic photovoltaics. *Nature* **2013**, *500* (7463), 435–439.
- (61) Menke, S. M.; Sadhanala, A.; Nikolka, M.; Ran, N. A.; Ravva, M. K.; Abdel-Azeim, S.; Stern, H. L.; Wang, M.; Sirringhaus, H.; Nguyen, T. Q.; Bredas, J. L.; Bazan, G. C.; Friend, R. H. Limits for Recombination in a Low Energy Loss Organic Heterojunction. *ACS Nano* **2016**, *10* (12), 10736–10744.
- (62) Kan, B.; Feng, H. R.; Wan, X. J.; Liu, F.; Ke, X.; Wang, Y. B.; Wang, Y. C.; Zhang, H. T.; Li, C. X.; Hou, J. H.; Chen, Y. S. Small-Molecule Acceptor Based on the Heptacyclic Benzodi-(cyclopentadithiophene) Unit for Highly Efficient Nonfullerene Organic Solar Cells. J. Am. Chem. Soc. 2017, 139 (13), 4929–4934.
- (63) Veldman, D.; Meskers, S. C. J.; Janssen, R. A. J. The Energy of Charge-Transfer States in Electron Donor-Acceptor Blends: Insight into the Energy Losses in Organic Solar Cells. *Adv. Funct. Mater.* **2009**, *19* (12), 1939–1948.
- (64) Jin, Y. Z.; Zhang, Y. X.; Liu, Y. F.; Xue, J.; Li, W. W.; Qiao, J.; Zhang, F. L. Limitations and Perspectives on Triplet-Material-Based Organic Photovoltaic Devices. *Adv. Mater.* **2019**, *31* (22), No. 1900690.
- (65) Liu, Z. Y.; Lu, T.; Chen, Q. X. An sp-hybridized all-carboatomic ring, cyclo[18]carbon: Electronic structure, electronic spectrum, and optical nonlinearity. *Carbon* **2020**, *165*, 461–467.
- (66) Guido, C. A.; Cortona, P.; Mennucci, B.; Adamo, C. On the Metric of Charge Transfer Molecular Excitations: A Simple Chemical Descriptor. *J. Chem. Theory Comput.* **2013**, *9* (7), 3118–3126.
- (67) Ghosh, D.; Kosenkov, D.; Vanovschi, V.; Flick, J.; Kaliman, I.; Shao, Y. H.; Gilbert, A. T. B.; Krylov, A. I.; Slipchenko, L. V. Effective fragment potential method in Q-CHEM: A guide for users and developers. J. Comput. Chem. 2013, 34 (12), 1060–1070.
- (68) Niu, Y.; Li, W.; Peng, Q.; Geng, H.; Yi, Y.; Wang, L.; Nan, G.; Wang, D.; Shuai, Z. MOlecular MAterials Property Prediction Package (MOMAP) 1.0: a software package for predicting the luminescent properties and mobility of organic functional materials. *Mol. Phys.* **2018**, *116* (7–8), 1078–1090.
- (69) Shuai, Z. Thermal Vibration Correlation Function Formalism for Molecular Excited State Decay Rates. *Chin. J. Chem.* **2020**, 38 (11), 1223–1232.
- (70) Wijsboom, Y. H.; Patra, A.; Zade, S. S.; Sheynin, Y.; Li, M.; Shimon, L. L. W.; Bendikov, M. Controlling Rigidity and Planarity in Conjugated Polymers: Poly(3,4-ethylenedithioselenophene). *Angew. Chem., Int. Ed.* **2009**, *48* (30), 5443–5447.

- (71) Bag, S.; Friederich, P.; Kondov, I.; Wenzel, W. Concentration dependent energy levels shifts in donor-acceptor mixtures due to intermolecular electrostatic interaction. *Sci. Rep.* **2019**, *9*, No. 12424. (72) Janssen, R. A. J.; Hummelen, J. C.; Wudl, F. Photochemical Fulleroid To Methanofullerene Conversion Via the Di-Pi-Methane (Zimmerman) Rearrangement. *J. Am. Chem. Soc.* **1995**, *117* (1), 544—
- (73) Hopper, T. R.; Qian, D. P.; Yang, L. Y.; Wang, X. H.; Zhou, K.; Kumar, R.; Ma, W.; He, C.; Hou, J. H.; Gao, F.; Bakulin, A. A. Control of Donor-Acceptor Photophysics through Structural Modification of a "Twisting" Push-Pull Molecule. *Chem. Mater.* **2019**, *31* (17), 6860–6869.
- (74) Kraner, S.; Scholz, R.; Plasser, F.; Koerner, C.; Leo, K. Exciton size and binding energy limitations in one-dimensional organic materials. *J. Chem. Phys.* **2015**, *143* (24), No. 244905.
- (75) Zhao, Z. W.; Pan, Q. Q.; Geng, Y.; Wu, Y.; Zhao, L.; Zhang, M.; Su, Z. M. Theoretical Insight into Multiple Charge-Transfer Mechanisms at the P3HT/Nonfullerenes Interface in Organic Solar Cells. ACS Sustainable Chem. Eng. 2019, 7 (24), 19699–19707.
- (76) Yao, H. F.; Cui, Y.; Qian, D. P.; Ponseca, C. S.; Honarfar, A.; Xu, Y.; Xin, J. M.; Chen, Z. Y.; Hong, L.; Gao, B. W.; Yu, R. N.; Zu, Y. F.; Ma, W.; Chabera, P.; Pullerits, T.; Yartsev, A.; Gao, F.; Hou, J. H. 14.7% Efficiency Organic Photovoltaic Cells Enabled by Active Materials with a Large Electrostatic Potential Difference. *J. Am. Chem. Soc.* 2019, 141 (19), 7743–7750.
- (77) Mothy, S.; Guillaume, M.; Ide, J.; Castet, F.; Ducasse, L.; Cornil, J.; Beljonne, D. Tuning the Interfacial Electronic Structure at Organic Heterojunctions by Chemical Design. *J. Phys. Chem. Lett.* **2012**, 3 (17), 2374–2378.